Journal of Systems Engineering and Electronics
Vol. 34, No. 6, December 2023, pp.1473 – 1482

Electric-controlled metasurface antenna array with ultra-wideband frequency reconfigurable reflection suppression

ZHENG Yuejun*, CHEN Qiang, DING Liang, YUAN Fang, and FU Yunqi

College of Electronic Science and Technology, National University of Defense Technology, Changsha 410073, China

Abstract: The electric-controlled metasurface antenna array (ECMSAA) with ultra-wideband frequency reconfigurable reflection suppression is proposed and realized. Firstly, an electric-controlled metasurface with ultra-wideband frequency reconfigurable in-phase reflection characteristics is designed. The element of the ECMSAA is constructed by loading the single electric-controlled metasurface unit on the conventional patch antenna element. The radiation properties of the conventional patch antenna and the reflection performance of electric-controlled metasurface are maintained when the antenna and the metasurface are integrated. Thus, the ECMSAA elements have excellent radiation properties and ultra-wideband frequency reconfigurable in-phase reflection characteristics simultaneously. To take a further step, a 6×10 ECMSAA is realized based on the designed metasurface antenna element. Simulated and measured results prove that the reflection of the ECMSAA is dynamically suppressed in the P and L bands. Meanwhile, high-gain and multi-polarization radiation properties of the ECMSAA are achieved. This design method not only realizes the frequency reconfigurable reflection suppression of the antenna array in the ultra-wide frequency band but also provides a way to develop an intelligent low-scattering antenna.

Keywords: electric-controlled metasurface antenna array (ECMSAA), radiation, reflection, frequency reconfigurable.

DOI: 10.23919/JSEE.2022.000121

1. Introduction

Metasurfaces (MSs) are planar surfaces constructed by periodic or quasi-periodic structures. Excellent and unique characteristics are the soul of the MSs. These characteristics can be obtained through flexible designs and elaborate arrangements of the MSs units [1−4]. Thus, the MSs attract focus investigations [5−8] and extensive applications [9−15], such as reflection suppression [9−13], polarization rotation and beam steering [14−15]. As a promising application, the MSs are utilized to reduce the reflection of an antenna [16−19] or antenna array, such as patch array [20−22], slot array [23], and phase array antenna [24−27]. The reflection of the antenna array is reduced by loading asymmetric structured MS [23]. Although the reflection of the antenna array is reduced by applying the MS, the challenges still exist [28]. The reflection suppression and radiation properties of antenna array are difficult to control simultaneously.

The design concept of MSs is introduced into antenna design to overcome the above challenges. The MS antenna owns radiation and reflection properties simultaneously. Two different MS antenna elements with in-phase reflection characteristics are utilized to construct the MS antenna array, and good reflection suppression and radiation properties are achieved simultaneously [29, 30]. The MS antenna elements are designed based on phase cancellation principle to obtain reflection suppression performance. Both the elements own in-phase reflection characteristics. The broadband reflection suppression is obtained when phase difference of the elements between 150° and 210° [10, 28]. The anisotropic structures of the antenna array are utilized. The antenna array is formed by using one kind of MS antenna elements. The reflection suppression and circular-polarized radiation performance are achieved [31]. However, the antenna influences the reflection suppression, and the suppression bandwidth is limited by the working frequency band of the antenna.

In this paper, an electric-controlled MS antenna array (ECMSAA) with ultra-wideband frequency reconfigurable reflection suppression is proposed and realized. Single MS unit and conventional patch antenna element are combined to form elements of the ECMSAA. The elements of the ECMSAA own frequency reconfigurable in-

Manuscript received November 08, 2021.
*Corresponding author.
This work was supported by the National Natural Science Foundation of China (61901493;61901492;61801485), and the Natural Science Foundation of Hunan Province (2020JJ5676).

phase reflection characteristics in the P and L bands and excellent radiation properties simultaneously. Moreover, the reflection properties and the radiation performance of the ECMSAA element can be controlled independently. A 6×10 ECMSAA is realized based on the novel designed element. The reflection of ECMSAA is dynamically suppressed in the P and L bands. Meanwhile, high-gain and multi-polarization radiation properties of the ECMSAA are achieved.

2. Design of ECMSAA element

As Fig. 1 presents, the designed ECMSAA element is composed of a single electric-controlled MS unit and a conventional patch antenna element. The MS and the antenna share the same metallic ground plane and dielectric substrate. The dielectric substrate is polyimide fiberglass cloth laminate TB-73 (ε =2.65, tan δ =0.006 7, p = 76, t =5 mm). The designed notched square ring and square radiation patch are etched on the top surface of the dielectric substrate. The square radiation patch (length=36 mm) is placed in the central area. Two feeding ports (with central deviation position of 7.2 mm) are used to achieve orthometric polarizations. Feeding port 1 deviates central position in the x-axis direction, while feeding port 2 deviates the central position in the y-axis direction. The notched square ring (square ring length= 75 mm, notch length=14 mm, notch width=7.5 mm) is placed around the radiation patch. Varactor diodes (SMV1265-011LF) are utilized on the notched square ring for adjusting reflection characteristics. One end of the varactor diode is concatenated to the ground plane through a metal column to increase the adjustment range. A strong current will flow through the varactor diode by introducing a short-circuited point. It is expected to achieve wideband frequency reconfigurable in-phase reflection characteristics.

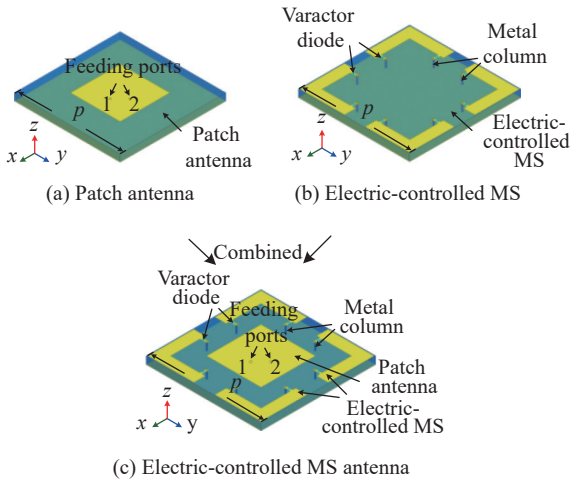

Fig. 1 Schematic geometry and forming process of the ECMSAA elements

To analyze the principle of electric-controlled MS, the reflection characteristics of the electric-controlled MS are investigated at the arbitrarily selected capacitance value (1.0 pF), shown in Fig. 2. The in-phase reflection at 1.04 GHz and 1.85 GHz are achieved, respectively.

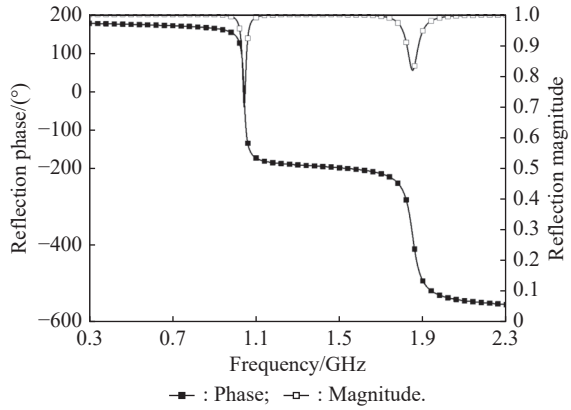

Fig. 2 Reflection characteristics of electric-controlled MS unit

The reflection magnitudes are slightly decreased. For further investigation, the surface current distributions of the electric-controlled MS unit are studied at 1.04 GHz and 1.85 GHz, depicted in Fig. 3.

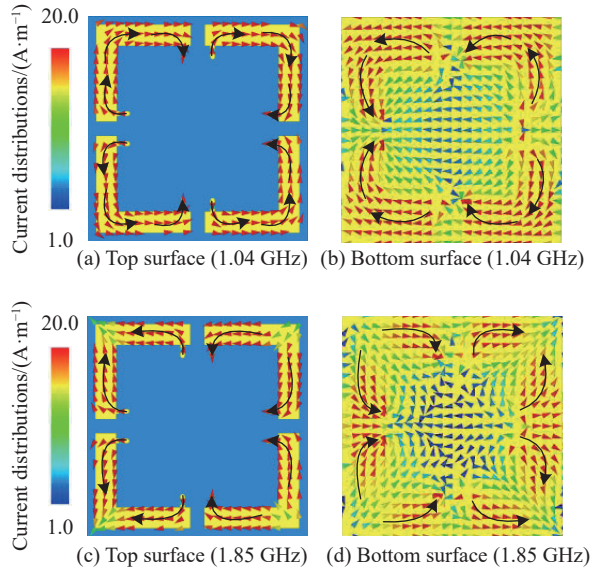

Fig. 3 Surface current distributions of electric-controlled MS unit at 1.04 GHz and 1.85 GHz

Intense current flow through the diode is observed. The intense current is produced at the short-circuited position. Due to intense current flow through the varactor diode, the reflection characteristics of the electric-controlled MS could be adjusted in a wide frequency range. Moreover, the induced current flow from one short-circuited position to another short-circuited position of the 1/4 notched square ring structure (“L” shape) at 1.04 GHz, shown in Fig. 3(a) and Fig. 3(b). Nevertheless, the induced current

both flow from short-circuited position to the central position of the 1/4 notched square ring structure ("L" shape) at 1.85 GHz, presented in Fig. 3(c) and Fig. 3(d). Thus, the MS possesses in-phase reflection at two frequencies and obtains wideband reconfigurable in-phase reflection characteristics.

Radiation and reflection properties of the designed ECMSAA element are investigated [28], shown in Fig. 2. Also, the performance of primary patch antenna element is taken as a comparison. As Fig. 4 shows, the radiation properties are studied at the four different capacitance values c (0.71 pF(minimum), 1.86 pF, 5.15 pF, and 17.41 pF (maximum)). The curves of the ECMSAA element at these four different capacitance values coincide well with the curves of the primary conventional patch antenna element. The ECMSAA element operates from 1.88 GHz to 1.97 GHz (reflection coefficient $|S_{11}|$ <−10 dB) and resonates at 1.91 GHz, depicted in Fig. 4(a). Good impedance matching is obtained. Moreover, transmission coefficient $|S_{21}|$ less than −32 dB at the working frequency band, indicating that good isolation is obtained between the two feeding ports. The 2D radiation patterns at 1.91 GHz of the ECMSAA element are depicted in Fig. 4(b) and Fig. 4(c). The main-beam patterns of the antenna are observed in the normal direction. The maximum gain is 6.16 dBi. The cross-polarization level of the antenna is 36.16 dB lower than the main-polarization level. Good radiation properties are maintained when the MS and the antenna are integrated. Moreover, the radiation properties are also kept when the capacitances of varactor diode of MS are changed. It can be concluded that the ECMSAA element achieves good radiation performance. Also, the radiation performance is well maintained when the reflection characteristics are changed. That is to say, the reflection characteristics of the ECMSAA element almost have no effect on the radiation properties.

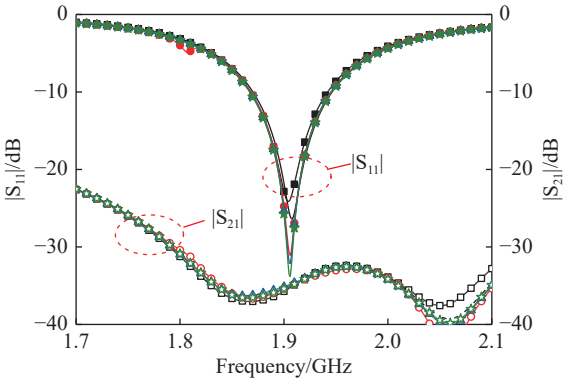

(a) Comparison of $|S_{11}|$ and $|S_{21}|$

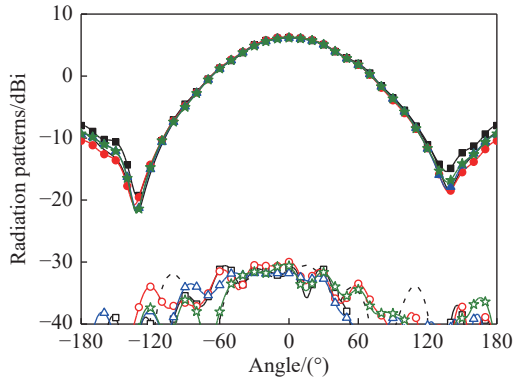

(b) Comparison of *xoz* plane radiation patterns

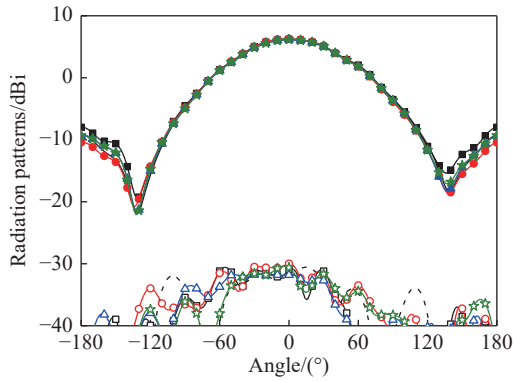

(c) Comparison of *yoz* plane radiation patterns

- - - : Primary; : c=0.71 pF; : c=1.86 pF; : c=5.15 pF; : c=17.41 pF.

Fig. 4 Radiation properties comparison of primary patch antenna element and ECMSAA element

The reflection characteristics of the ECMSAA element are also investigated at the same four different capacitance values (0.71 pF, 1.86 pF, 5.15 pF, and 17.41 pF), depicted in Fig. 5. The reflection characteristics of the primary electric-controlled MS unit are taken as a comparison. The curves of the ECMSAA element at four different capacitance values almost agree with the curves of the primary electric-controlled MS unit. The in-phase reflection characteristics are dynamically adjusted in the P and L bands. The slope of the reflection phase is positive in the operation band of the antenna. Meanwhile, the reflection magnitude is sharply reduced due to the 50 Ω impedance matching absorption of the antenna. The absorbing characteristics are helpful to suppress reflection. It can be concluded that the ECMSAA element achieves ultra-wideband frequency reconfigurable in-phase reflection characteristics. Meanwhile, it also can be indicated that patch antenna may have little influence on MS.

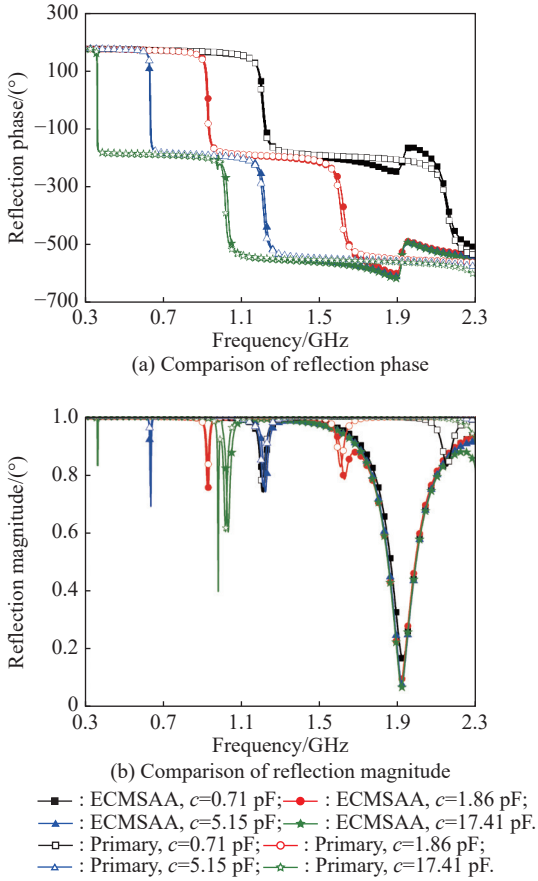

Fig. 5 Reflection characteristics comparison of primary MS unit and ECMSAA element

To further analyze the influence of patch antenna, the reflection characteristics of ECMSAA elements in the operation band are investigated. The reflection phase and magnitude of ECMSAA element at the five different capacitance values (0.91 pF, 0.97 pF, 1.05 pF, 1.12 pF, and 1.30 pF) are depicted in Fig. 6. The in-phase reflection characteristics are obtained in the operation band. Moreover, the in-phase reflection characteristics can be dynamically adjusted. As Fig. 6(b) presents, the magnitude of reflection is sharply reduced in the operation band while the magnitude of reflection is higher than 0.8 for some capacitance values.

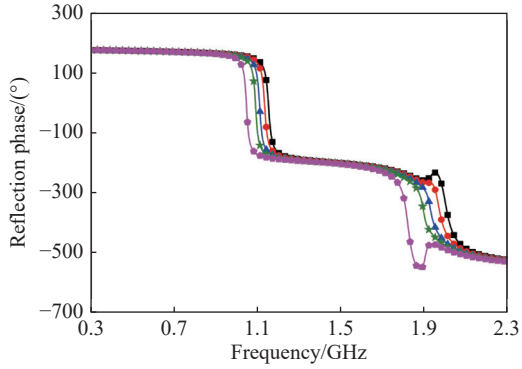

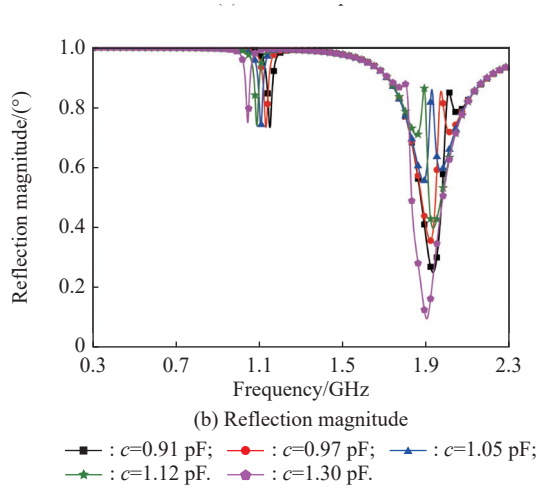

Fig. 6 Reflection characteristics of ECMSAA element in the operation band

To analyze the reasons that the reflection magnitude is higher than 0.8, the reflection magnitude of the ECMSAA element at the capacitance values 1.05 pF is selected, and the surface current distributions at 1.92 GHz (the reflection magnitude is higher than 0.8) and 1.97 GHz (the reflection magnitude is lower than 0.8) are investigated and shown in Fig. 7.

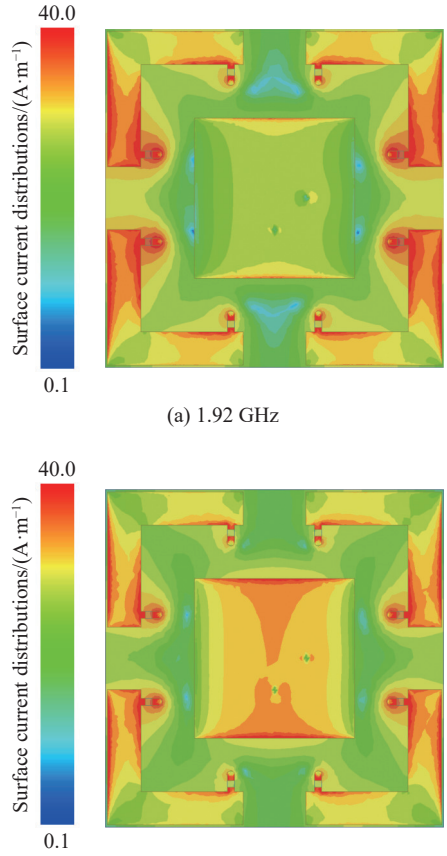

Fig. 7 Surface current distributions of ECMSAA element at the capacitance values 1.05 pF

As Fig. 7(a) presents, the intense induced current is observed on the MS at 1.92 GHz. Most of the incidence is reflected by the MS. As Fig. 7(b) shows, the intense induced current is observed on the MS and patch antenna at 1.97 GHz. The incidence is reflected by the MS and is absorbed by the patch antenna. Thus, the magnitude of reflection is higher than 0.8 at 1.92 GHz and is lower than 0.8 at 1.97 GHz. From the above analysis, the magnitude of reflection higher than 0.8 is mainly produced by the MS. Meanwhile, the small rest portion of the incidence is absorbed by the antenna. The absorption of the antenna is helpful to suppress reflection. It can be concluded that the antenna almost has no influence on the MS. It is further demonstrated that the reflection and radiation performance of the ECMSAA element can be controlled independently.

3. Design and performance of ECMSAA

A 6×10 ECMSAA is realized based on the novel designed element, shown in Fig. 8. Since the ECMSAA element owns two feeding ports and the ports can be fed independently. The ECMSAA is expected to radiate multi-polarized waves [28].

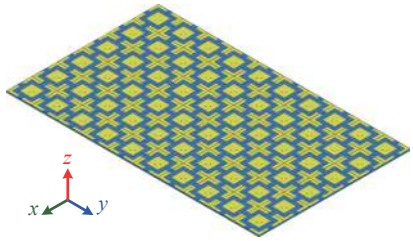

Fig. 8 Schematic geometry of the 6×10 ECMSAA

The radiation properties of ECMSAA are investigated based on the feeding solution [28]. Firstly, only the feeding port 1 is fed, and the feeding phase is 0°. The radiation performance of ECMSAA are investigated and depicted in Fig. 9. To describe the $|S_{11}|$ of ECMSAA, four elements of ECMSAA are casually selected. The ECMSAA elements resonate close to 1.895 GHz, and good impedance matching is achieved as shown in Fig. 9(a). 2D radiation patterns at resonant frequency are presented in Fig. 9(b). The ECMSAA radiates forward, and the maximum gain reaches 22.2 dBi. The maximum cross-polarization level value is 39.3 dB lower than that of main-polarization. Electric field distributions are studied on the $8\lambda_{1.895\ \mathrm{GHz}}$ surface above the ECMSAA. As Fig. 9(c) shows, the direction of the electric field is along the x-axis direction. Thus, it can be concluded that the ECMSAA owns good radiation performance and radiates x-polarized waves. The above analysis infers that ECMSAA also owns the ability to radiate y-polarized waves when feeding port 2 is fed, and the feeding phase is 0°.

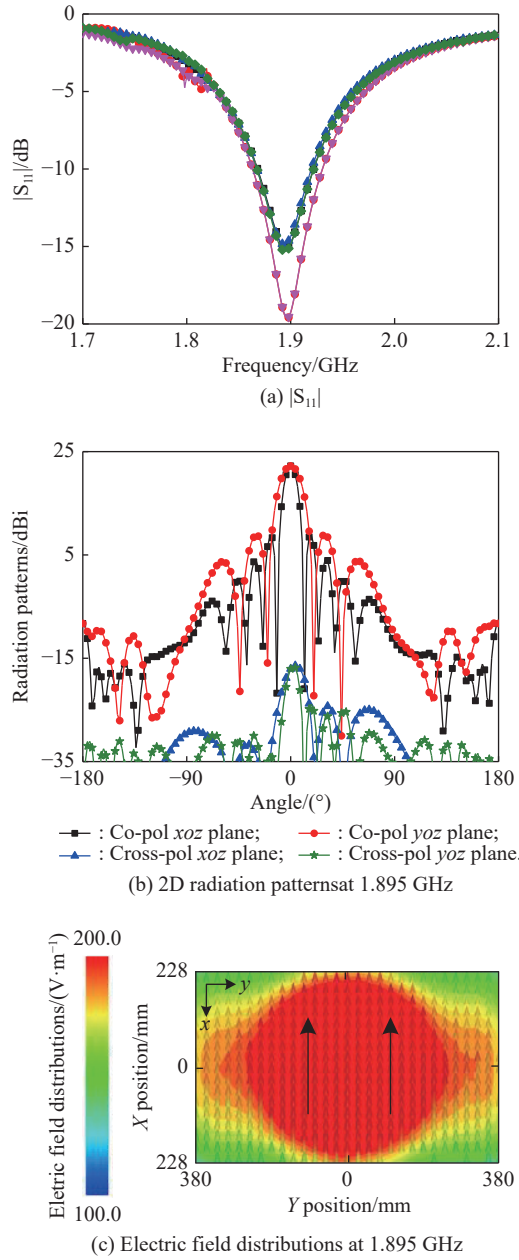

Fig. 9 x-polarized radiation properties of ECMSAA

Take a further step, the feeding port 1 and port 2 are both fed. The feeding phase of port 1 is 90° and feeding phase of port 2 is 0°. The radiation performance of the ECMSAA is studied and presented in Fig. 10. To describe the reflection coefficients $|S_{22}|$ of the ECMSAA, four elements of the ECMSAA are casually selected. As Fig. 10(a) shows, the elements of the ECMSAA resonate close to 1.895 GHz, and good impedance matching is achieved. 2D radiation patterns of the ECMSAA at resonant frequency are shown in Fig. 10(b). ECMSAA radiates forward, and the maximum gain reaches 21.8 dBi. The axial ratio of the ECMSAA is 0.26 dB in the operation band, shown in Fig. 10(c). Electric field distribu-

tions are investigated on the $8\lambda_{1.895\ \mathrm{GHz}}$ surface above the ECMSAA at four different moments in a period. As Fig. 10(d) shows, the direction of the electric field rotates counterclockwise, that is, following the right-hand law. From the above analysis, it can be concluded that the ECMSAA owns good radiation performance and radiates the right circular-polarized waves. It can also infer that ECMSAA radiates left circular-polarized waves when the port 1 and port 2 are fed, and the feeding phases of port 1 and port 2 are 0° and 90°, respectively. Moreover, the ECMSAA also possesses the ability to radiate elliptical-polarized waves.

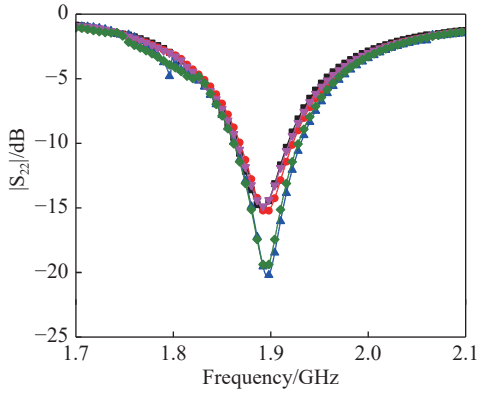

(a) $|S_{22}|$

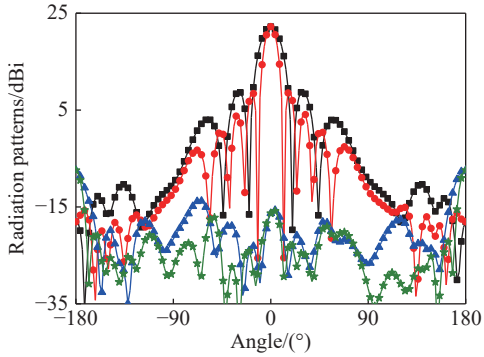

(b) 2D radiation patterns at 1.895 GHz

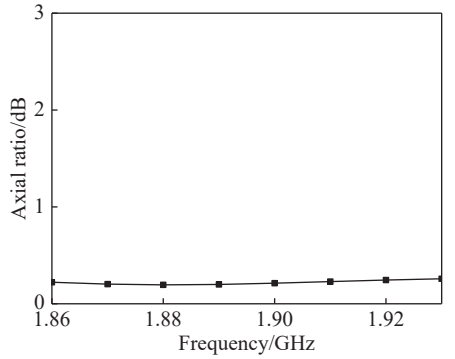

(c) Axial ratio

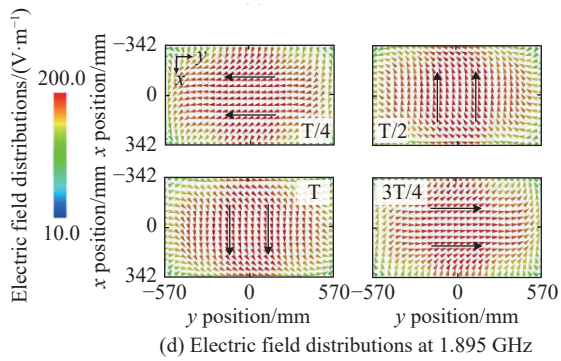

(d) Electric field distributions at 1.895 GHz

Fig. 10 Right circular-polarized radiation properties of ECMSAA

To investigate the adjustable reflection suppression performance, the ECMSAA is divided into arrays, shown in Fig. 11. According to the classic checkerboard arrangement, the 6×10 antenna array is divided into four 3×5 E1 and E2 small arrays.

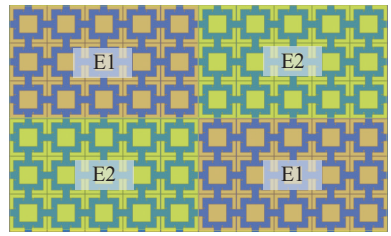

Fig. 11 Division of ECMSAA

The reflection phase of ECMSAA element at the five different capacitance values (0.83 pF, 0.91 pF, 2.60 pF, 2.70 pF, and 3.00 pF) are selected and studied, presented in Fig. 12(a). The ECMSAA element owns dual 0° reflection phases. The reflection phase curves of the ECMSAA elements in the E1 and E2 areas are close to each other, which is beneficial to achieve effective phase difference (150°−210°). As Fig. 12(b) shows, the phase difference of the elements under 0.83 pF and 0.91 pF meet the effective phase difference condition in the high- and low-frequency range. However, the phase difference of the elements under 2.7 pF and 3.0 pF meet the effective phase difference condition in the high-frequency range, and the phase difference of the elements under 2.6 pF and 2.7 pF meet the effective phase difference condition in the low-frequency range. Due to the ECMSAA could be treated as the MS, a same size metallic plane is taken as a comparison [28], plotted in Fig. 12(c). Remarkable reflection suppression of the ECMSAA is achieved for normal incidence. Moreover, as the capacitance value increases, the reflection suppression band shifts to low frequency, which coincides with the changing trend of the reflection phase of the ECMSAA elements. The reflection reduction of the ECMSAA for oblique incidence is shown in Fig. 12(d). The reflection suppression band is casually selected. Although the incidence increases to 45°, the ECMSAA also owns the ability to suppress the reflection.

From the above analysis, it can be concluded that the reflection can be dynamically suppressed in an ultra-wide frequency range covering the P and L bands by adjusting the varactor diode. Out-of-band and in-band reflection reduction of the ECMSAA are obtained, and the flexibility of reflection suppression is improved.

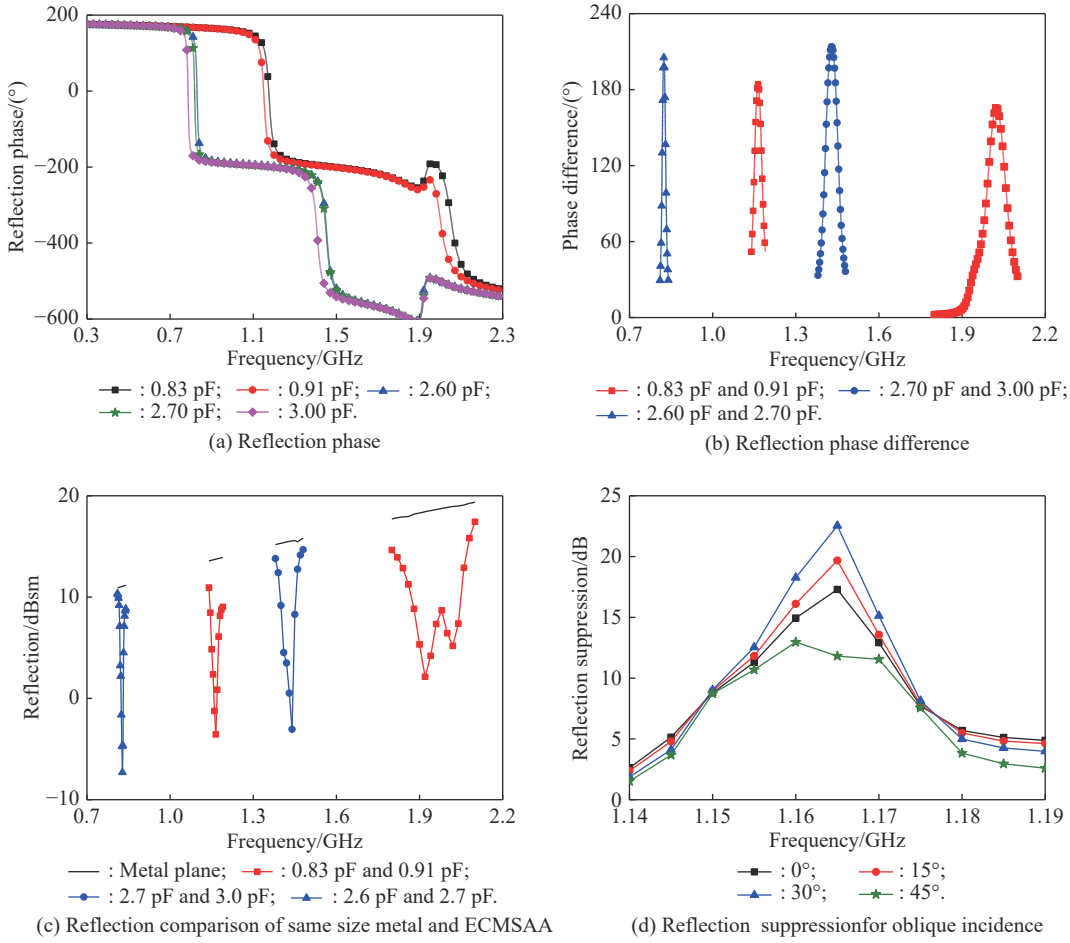

(a) Reflection phase

(b) Reflection phase difference

(c) Reflection comparison of same size metal and ECMSAA

(d) Reflection suppressionfor oblique incidence

Fig. 12 Reflection suppression performance of ECMSAA

4. Fabrication and measurement

To further verify the design method, the sample of the ECMSAA is fabricated and measured, presented in Fig. 13. Due to many array elements, several elements are randomly selected to investigate the reflection coefficient, presented in Fig. 14(a) and Fig. 14(b). The ECMSAA elements resonate close to 1.87 GHz, and good impedance matching is achieved. The *xoz* plane radiation patterns at 1.87 GHz are shown in Fig. 14(c). The ECMSAA radiates forward. The beamwidth of the ECMSAA is narrow, and the directivity is good. The sidelobe level is below −10.5 dB, and the maximum cross-polarization level is less than −30.6 dB. From the above results, it can be concluded that the ECMSAA owns good radiation performance.

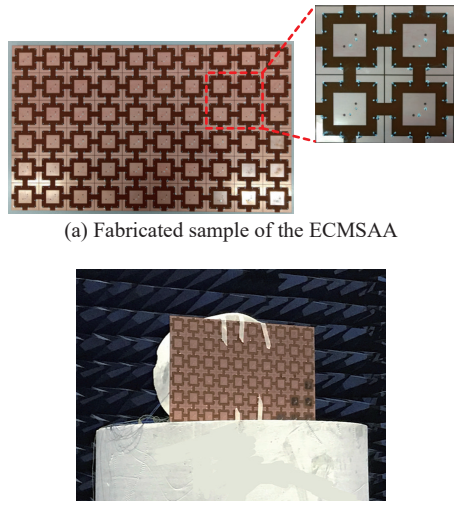

(a) Fabricated sample of the ECMSAA

(b) Measurement configuration of the ECMSAA

Fig. 13 Sample and measurement configuration of the ECMSAA

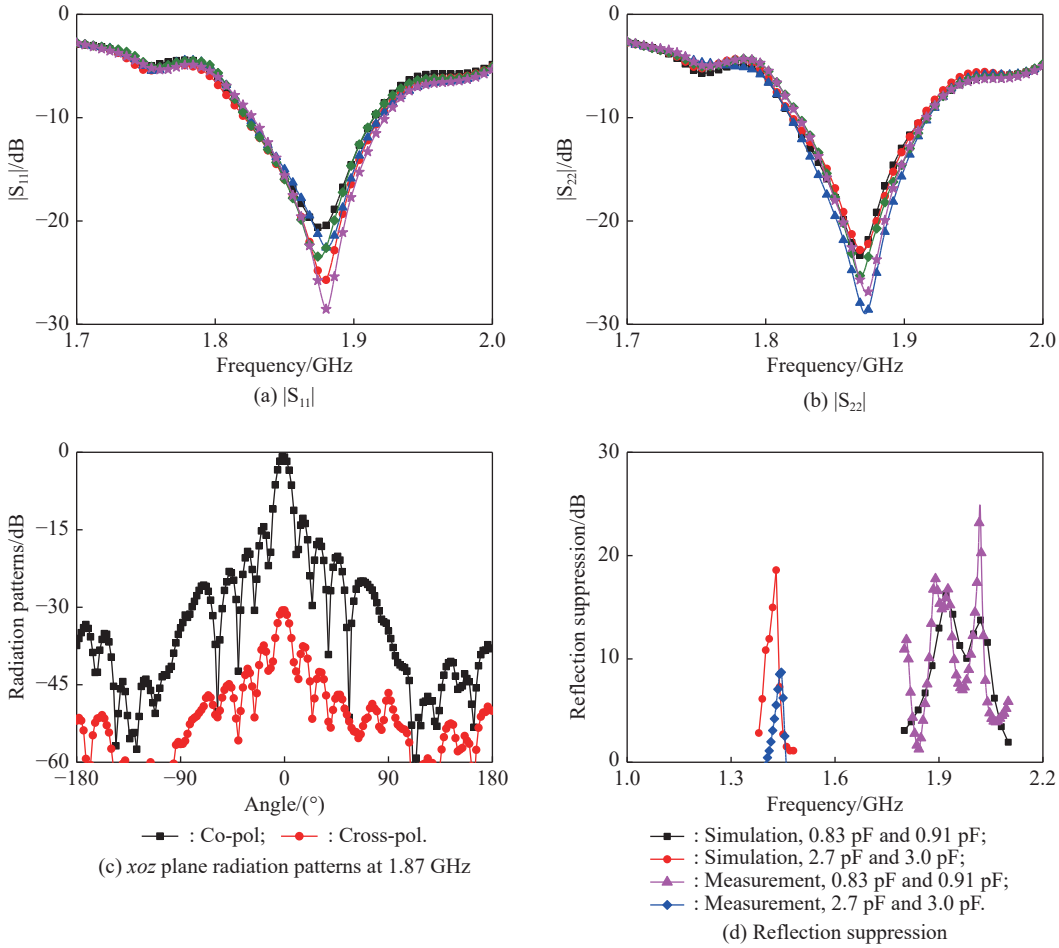

Fig. 14 Radiation properties and reflection suppression performance of the ECMSAA

Due to the limited experimental conditions, the reflection suppression is measured in the high-frequency range. As Fig. 14(d) shows, the measurements are basically consistent with the simulations. The reflection suppression amplitude is dropped, and the suppression bandwidth is also narrowed when the capacitance values are 2.7 pF and 3.0 pF. The deviation may be caused by the limited anechoic chamber space. It fails to meet the far-field conditions well, which affects the reflection phase of the elements. The measurement results verifiy that the reflection of ECMSAA can be dynamically suppressed in the P and L bands.

5. Conclusions

In view of the problem that the reflection suppression bandwidth of MS antenna array is limited by antenna working bandwidth, an electric-controlled MS antenna array is proposed. The single electric-controlled MS unit and conventional patch antenna element are combined to form an element of ECMSAA. The element of ECMSAA owns excellent radiation properties and ultra-wideband frequency reconfigurable in-phase reflection characteristics. Moreover, the reflection and radiation properties of the ECMSAA elements could be controlled independently. The 6×10 ECMSAA is realized and fabricated based on the designed ECMSAA element. The measured and simulated results both show that the ECMSAA possesses good radiation properties and owns dynamical reflection suppression in the P and L bands. Out-of-band and in-band reflection suppression of the ECMSAA are achieved, and the flexibility of the reflection suppression is improved.

References

[1] GUO M, SUN Z S, SANG D, et al. Design of frequency-selective rasorbers based on centrosymmetric bended-strip resonator. IEEE Access, 2019, 7: 24964–24970.

[2] LANDY N I, SAJUYIGBE S, MOCK J J, et al. Perfect metamaterial absorber. Physical Review Letters, 2008, 100: 207402.

[3] PAQUAY M, IRIARTE J C, EDERRA I, et al. Thin AMC structure for radar cross-section reduction. IEEE Trans. on Antennas and Propagation, 2007, 55(12): 3630–3638.

[4] CAI T, WANG G M, ZHANG X F, et al. Compact microstrip antenna with enhanced bandwidth by loading magneto-elec-

tro-dielectric planar waveguided metamaterials. IEEE Trans. on Antennas and Propagation, 2015, 63(5): 2306–2311.
[5] JIA Y T, LIU Y, GONG S X, et al. Broadband polarization rotation reflective surfaces and their applications to RCS reduction. IEEE Trans. on Antennas and Propagation, 2016, 64(1): 179–188.
[6] YANG H H, CAO X Y, YANG F, et al. A programmable metasurface with dynamic polarization, scattering and focusing control. Scientific Reports, 2016, 6: 35692.
[7] LIU S, CUI T J, XU Q, et al. Anisotropic coding metamaterials and their powerful manipulation of differently polarized terahertz waves. Light: Science and Applications, 2016, 5(1): e16076.
[8] HONG T, WANG S, GONG S X, et al. RCS reduction and gain enhancement for the circularly polarized array by polarization conversion metasurface coating. IEEE Antenna and Wireless Propagation Letters, 2019, 18(1): 167–171.
[9] CHEN Q, SANG D, GUO M, et al. Miniaturized frequency selective rasorber with a wide transmission band using circular spiral resonator. IEEE Trans. on Antennas and Propagation, 2019, 67(2): 1045–1052.
[10] YUAN F, XU H X, FU Y Q, et al. RCS reduction based on concave/convex-chessboard random parabolic-phased metasurface. IEEE Trans. on Antennas and Propagation, 2020, 68(3): 2463–2468.
[11] ORUJI A, PESARAKLOO A, KHALAJ-AMIRHOSSEINI M, et al. Ultrawideband and omnidirectional RCS reduction by using symmetrical coded structures. IEEE Antenna and Wireless Propagation Letters, 2020, 19(7): 1236–1240.
[12] WANG Y, CHEN K, LI Y, et al. Design of non-resonant metasurfaces for broadband RCS reduction. IEEE Antennas and Wireless Propagation Letters, 2021, 20(3): 346–350.
[13] SAMADI F, SEBAK A. Widebandvery low RCS engineered surface with a wide incident angle stability. IEEE Trans. on Antennas and Propagation, 2020, 69(3): 1809–1814.
[14] MA X L, HUANG C, LUO X G, et al. Single layer circular polarizer using metamaterial and its application in antenna. Microwave and Optical Technology Letters, 2012, 54(7): 1770–1774.
[15] JI L Y, GUO Y J, GONG S X, et al. A reconfigurable partially reflective surface (PRS) antenna for beam steering. IEEE Trans. on Antennas and Propagation, 2015, 63(6): 2387–2395.
[16] ZHENG Y J, GAO J, CAO X Y, et al. Wideband RCS reduction of a microstrip antenna using artificial magnetic conductor structures. IEEE Antenna and Wireless Propagation Letters, 2015, 14: 1582–1585.
[17] ZHAO Y, CAO X Y, GAO J, et al. Broadband low-RCS metasurface and its application on antenna. IEEE Trans. on Antennas and Propagation, 2016, 64(7): 2954–2962.
[18] ZHENG Y J, GAO J, CAO X Y, et al. Wideband gain enhancement and RCS reduction of fabry-perot resonator antenna with chessboard arranged metamaterial superstrate. IEEE Trans. on Antennas and Propagation, 2018, 54(2): 590–598.
[19] SHI Y, MENG Z K, WEI W Y, et al. Characteristic mode cancellation method and its application for antenna RCS reduction. IEEE Antenna and Wireless Propagation Letters, 2019, 18(9): 1784–1788.
[20] LIU Z M, LIU S B, ZHAO X, et al. Wideband gain enhancement and RCS reduction of fabry–perot antenna using hybrid reflection method. IEEE Trans. on Antennas and Propagation, 2020, 68(9): 6497–6505.
[21] YANG H H, LI T, XU L M, et al. Low in-band-RCS antennas based on anisotropic metasurface using a novel integration method. IEEE Trans. on Antennas and Propagation, 2021, 69(3): 1239–1248.
[22] JIA Y T, LIU Y, FENG Y J, et al. Low-RCS holographic antenna with enhanced gain based on frequency-selective absorber. IEEE Trans. on Antennas and Propagation, 2020, 68(9): 6516–6525.
[23] LIU Y, LI K, JIA Y T, et al. Wideband RCS reduction of a slot array antenna using polarization conversion metasurfaces. IEEE Trans. on Antennas and Propagation, 2016, 64(1): 326–331.
[24] CHENG Y F, FENG J, LIAO C, et al. Analysis and design of wideband low-RCS wide-scan phased array with AMC ground. IEEE Antenna and Wireless Propagation Letters, 2021, 20(2): 209–213.
[25] PANDIT S, MOHAN A, RAY P. Low-RCS low-profile four-element MIMO antenna using polarization conversion metasurface. IEEE Antenna and Wireless Propagation Letters, 2020, 19(12): 2102–2106.
[26] MENG Z K, SHI Y, WEI W Y, et al. Multifunctional scattering antenna array design for orbital angular momentum vortex wave and RCS reduction. IEEE Access, 2020, 8: 109289–109296.
[27] YIN L, YANG P, GAN Y Y, et al. A low cost, low in-band RCS microstrip phased-array antenna with integrated 2-bit phase shifter. IEEE Trans. on Antennas and Propagation, 2021, 69(8): 4517–4526.
[28] ZHENG Y J, DING L, CHEN Q, et al. Integrating electromagnetic surface and antenna array for reflection suppression and excellent radiation. Journal of Systems Engineering and Electronics, 2021, 32(3): 517–526.
[29] ZHENG Y J, CAO X Y, GAO J, et al. Integrated radiation and scattering performance of a multifunctional electromagnetic surface. Optics Express, 2017, 25(24): 3001–3012.
[30] LIU Y, JIA Y T, ZHANG W B, et al. An integrated radiation and scattering performance design method of low-RCS patch antenna array with different antenna elements. IEEE Trans. on Antennas and Propagation, 2019, 67(9): 6199–6204.
[31] FAN Y, WANG J F, LI Y F, et al. Low-RCS and high-gain circularly polarized metasurface antenna. IEEE Trans. on Antennas and Propagation, 2019, 67(12): 7197–7203.

Biographies

ZHENG Yuejun was born in 1989. He received his B.S., M.S., and Ph.D. degrees from Air Force Engineering University , Xi'an, China, in 2012, 2014, and 2018, respectively. In June 2018, he joined the faculty of the National University of Defense Technology, Changsha, China, where he is currently an associate professor. His research interests include microwave and optics metasurface, metasurface antenna, radiation and scattering integration technology. He has authored and coauthored more than 40 scientific papers in major journals and conferences.
E-mail: zhengyuejun18@nudt.edu.cn

CHEN Qiang was born in 1991. He received his B.S., M.S., and Ph.D. degrees from National University of Defense Technology, Changsha, China, in 2012, 2014, and 2018, respectively, where he is currently a lecturer. His current research interests include artificial electromagnetic materials, electromagnetic materials antenna, circuit analog absorbers, and frequency selective surface.
E-mail: chenqiang08a@nudt.edu.cn

DING Liang was born in 1985. He received his M.E. and Ph.D. degrees in electrical engineering from National University of Defense Technology, Changsha, China, in 2010 and 2014, respectively. From 2012 to 2014, he was a visiting researcher in the Electromagnetic Imaging Laboratory, University of Manitoba, Winnipeg, Canada. He is currently a lecturer with the College of Electronic Science and Technology, National University of Defense Technology. His main research interests include inverse problem, metasurfaces and microwave photonics.
E-mail: lio.dingliang@hotmail.com

YUAN Fang was born in 1992. He received his B.E. degree in Sichuan University in 2016, and his M.S. degree in Air Force Engineering University in 2019. He is currently pursuing his Ph.D. degree in electronic engineering at National University of Defense Technology, Changsha, China. His research interests include design of spatiotemporal metasurfaces and radar cross section reduction metasurface.
E-mail: 13379260913@163.com

FU Yunqi was born in 1975. He received his B.E. degree in 1997, M.S. degree in 2000, and Ph.D. degree in 2004, in electronic science and technology from National University of Defense Technology (NUDT), Changsha, China. His Ph.D. dissertation was awarded with the national excellent dissertation nomination paper and the provincial excellent doctoral dissertation of Hunan. From 2009 to 2010, he was a visiting scholar at Ohio State University, the U.S. Since 2011, he has been a professor with the NUDT. He was elected by the New Century Talent Supporting Project by education ministry in 2008. His current research interests include the metamaterial and metasurface, and microwave and millimeter-wave technology.
E-mail: yunqifu@nudt.edu.cn